Numerical Simulation and Structural Optimization Analysis of a Vortex Chamber Supercharge

Xingrong Wang*, Jiafei Pu
School of Mechanical Engineering, Huangshan University, Huangshan, Anhui, China
**Corresponding Author.*

Abstract:In order to enhance the efficiency and stability of the vortex chamber supercharger in conveying media, models of vortex chamber superchargers with different diameters were constructed. The FLUENT simulation software was employed to perform mesh generation and numerical simulation of the fluid domain, obtaining the internal fluid velocity, pressure distribution, and motion trajectories for each model. The fluid characteristics of different vortex chamber models were analyzed to identify their operational patterns. The results indicate that as the diameter of the vortex chamber increases, the working efficiency of the vortex chamber supercharger first increases and then decreases. When the diameter of the vortex chamber is 50 mm, a significant vortex phenomenon occurs in the area near the center of the vortex chamber, forming a distinct low-pressure zone and increasing the fluid velocity at the inlets on both sides of the axial direction. The average velocity at the inlets on both axial sides reaches its maximum value of 10.55 m/s, and the working efficiency is the highest at 17.7%.

Keywords: Vortex Chamber Supercharger; Numerical Simulation; Working Efficiency; Fluid Characteristics;

1. Introduction

pump is a mechanical device used to transport liquids or increase liquid pressure. It transfers the mechanical energy of a prime mover or other external energy to the liquid, thereby increasing the liquid's energy[1]. Pumps are mainly used to transport media such as water, oil, acid-base solutions, emulsions, and suspensions, and can also handle solid-liquid mixtures[2,3]. Based on their working principles, pumps are classified into three categories: positive displacement pumps, dynamic pumps, and other types of pumps[4]. They are widely used in fields such as chemical and petroleum industries, agriculture, mining, metallurgy, and water conservancy[5,6]. Different types of pumps are suitable for different working conditions and environments. The nature of the transported medium also determines the type of pump to be used. For example, when transporting corrosive, toxic, or abrasive media, traditional impeller pumps require high levels of sealing and stability[7,8], which not only increases transportation costs but also reduces pump performance and safety[9]. To address these issues, researchers have explored the use of jet pumps for medium transportation. Although jet pumps have a simple structure and can transport various media, their efficiency is relatively low. Wang Changbin et al.[10] studied the working principles of jet pumps and addressed issues such as low efficiency, high sensitivity, and susceptibility to cavitation by analyzing the impact of jet pump structural dimensions on turbulent jet flow fields, thereby improving the hydraulic characteristics of jet pumps. Sun Rui et al.[11] investigated the influence of structural design on the hydraulic performance of high-pressure rotary vane pumps, finding that excessively high pump shaft speeds can intensify internal component friction, affecting product performance and shortening the pump's service life.

Traditional jet pumps suffer from issues such as high discharge noise, numerous vulnerable parts, and high energy consumption. Additionally, the large throat length of jet pumps results in significant longitudinal dimensions[12], making them unsuitable for use in compact structures. To improve the reliability and stability of

liquid transportation, Rogovie A[13] proposed a novel vortex chamber supercharger. This supercharger, by adding a vortex chamber at the end of the transportation pump device, prevents direct contact between the pump and the transported medium, thereby avoiding corrosion and wear of internal pump components caused by bulk materials or chemical products.

At present, research efforts primarily focus on analyzing the internal fluid dynamics performance of supercharger pumps, while studies on the structural optimization and simulation design of new vortex chamber superchargers are limited. This paper focuses on analyzing the impact of internal structural dimensions of the vortex chamber supercharger on the fluid characteristics of the transported liquid medium. By establishing a three-dimensional simulation model and conducting numerical simulations of the flow field, the structural dimensions of the vortex chamber are optimized to enhance the efficiency and stability of medium pumping. This research aims to provide valuable foundational theoretical insights for solving practical engineering problems.

2. Three-Dimensional Model

As shown in Figure 1(a), the three-dimensional model structure of the vortex chamber supercharger is illustrated. The main body of the vortex chamber is cylindrical, with two axisymmetric channels opened at the circumferential edge. One of these channels serves as the pump's active flow path, while the other functions as the outlet flow path. The axial channels of the vortex chamber are two axial suction channels. When the pump transports liquid media, the fluid flows into the vortex chamber through the active flow path along the circumferential edge of the main body, forming a rotating vortex inside the vortex chamber. The centrifugal force increases the rotational speed, thereby creating a low-pressure zone in the axial center region. The resulting pressure difference drives the suction of media through the two axial channels, which is then ejected through the outlet flow path. The structural dimensions of the vortex chamber supercharger model are shown in Figure 1(b).

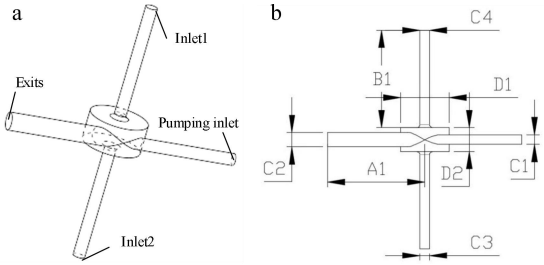

Figure 1. Structure of Vortex Chamber Turbocharger:
(a) Three Dimensional Model Structure of Vortex Chamber Supercharger;
(b) Structural Dimensions of Vortex Chamber Turbocharger Model

The specific dimensions of the vortex chamber supercharger are shown in Table 1.

Table 1. Dimensions of Vortex Chamber Turbocharger

Structure	Vortex chamber booster size/mm
Tangential channel length /A1	100
Axial channel /B1	100
Active channel diameter /C1	10
Outlet channel diameter /C2	15
Towards suction channel 1/C3	10
Axial suction channel 2/C4	10
Vortex chamber diameter /D1	50
Vortex chamber height /D2	30

3. Numerical Simulation

3.1 Control Equation

The most common indoor flow model is based on the Navier-Stokes equations, which are nonlinear second-order partial differential equations. Currently, they are among the most challenging hydrodynamic equations to solve. Written in their most compact form and neglecting body forces, the continuity equation is as follows[14]:

$$\begin{cases} \rho \dfrac{\partial \overline{V}}{\partial t} = Div\,(P - \rho \overline{V}\,\overline{V}); \\ P = -pE + 2\mu \dot{S}; \\ \dot{S}_{ij} = \dfrac{1}{2}\left(\dfrac{\partial V_i}{\partial x_j} + \dfrac{\partial V_j}{\partial x_i} \right); \\ div\,\overline{V} = 0. \end{cases} \tag{1}$$

Among them, ρ is the density of the medium; $\overline{V}$ is the vector of the current velocity at a given point in space; t is time; P is the stress tensor; $\dot{S}$ is a tensor of relative strain rate; p is the fluid dynamic pressure in viscous moving

fluids; E is a tensor unit; μ is the dynamic viscosity; Index $i = 1,2,3..., j = 1,2,3...$

3.2 Grid Settings

The vortex chamber supercharger uses a universal mesh template to generate tetrahedral meshes. The curvature normal angle is set to 11°, the minimum size adopts the default value of mesh generation at $1.5395e^{-4}$ m, the minimum edge length of the mesh is $3.146e^{-2}$ m, the transition ratio is set to 0.77, the maximum layer is set to 5, and the growth rate is set to 1.2. The "transition ratio" is set to 0.77, the "maximum layer" is set to 5, and the "growth rate" is set to 1.2. After the system automatically generates the mesh, the vortex chamber supercharger has a total of 302117 mesh elements. Mesh refinement is applied at the connections and edges of the model to ensure computational accuracy. The mesh of the fluid region of the vortex chamber supercharger is shown in Figure 2.

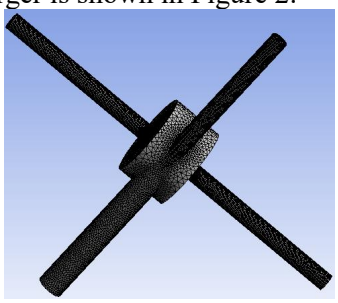

Figure 2. Grid Model of Vortex Chamber Turbocharger

3.3 Boundary Conditions

The pressure at the inlet and outlet of the vortex chamber pump is not constant, and the pressure difference between the inlet and outlet is one of the main factors determining the flow rate of the vortex chamber pump. Therefore, constant pressure boundary conditions are set at the inlet and outlet of the vortex chamber supercharger. The boundary condition for the supply channel is set to a total pressure of 2 MPa, the boundary condition for the outlet is set to a static pressure of 0 Pa, the pressure for the axial channel is set to 0 Pa, and the boundary condition for the wall is set to no-slip. The pressure variations in the outlet flow and supply flow are used as convergence criteria.

4. Analysis of Numerical Simulation Results

4.1 Transient Flow Rate of Each Channel

As shown in Figure 3, the transient boundary flow rate curves of each channel in the vortex chamber are illustrated. The flow rates of the two axial channels in the vortex chamber supercharger are identical, and the flow rate curves of the two axial channels in Figure 3 completely overlap. In the vortex chamber, the flow rate of each channel shows an increasing trend during the first 50 time steps. When the flow rate of each channel reaches a dynamic balance and stable state after 60 time steps, the axial pumping flow rate reaches its maximum value. Within the first 20 time steps, a backflow phenomenon occurs in the axial channels, primarily because when the pump starts operating, the liquid has just entered the vortex chamber from the tangential inlet, and a stable vortex has not yet formed inside the vortex chamber. As a result, a low-pressure zone is not established in the central region of the vortex chamber. When the vortex chamber becomes saturated with liquid, a brief backflow phenomenon occurs in the axial flow channels. Over time, the outlet flow rate increases. The flow in the pump's inlet channel, outlet channel, and axial channels tends to stabilize.

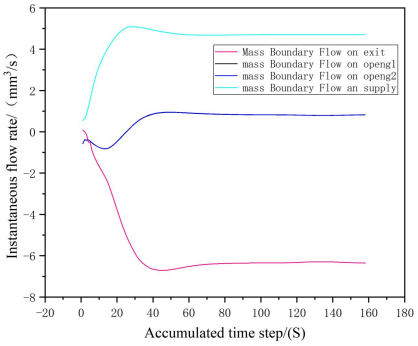

Figure 3. Transient Boundary Flow Curves of Each Channel in the Vortex Chamber

4.2 The Influence of Vortex Chamber Diameter on Its Working Efficiency

The vortex chamber supercharger primarily transports media into the vortex chamber through a delivery pump, forming a vortex under the action of centrifugal force. It demonstrates excellent performance in transporting solid particles, but its efficiency does not significantly improve when pumping low-density media such as water. The working efficiency of the vortex chamber supercharger is mainly influenced by the axial inflow velocity of the fluid and the magnitude of the

additional centrifugal force acting on the fluid. To enhance the transport efficiency of the vortex chamber supercharger for pumping fluids, the diameter of the vortex chamber was optimized. Based on the structure of the vortex chamber supercharger, five models with different vortex chamber diameters were designed, labeled as Model 1# to Model 6#. The diameters of the vortex chambers are 40 mm, 45 mm, 55 mm, 60 mm, and 65 mm, respectively. The impact of the internal structural dimensions of the vortex chamber supercharger on its working efficiency was analyzed through numerical simulation.

The relative centrifugal force depends on the rotational radius and speed of the fluid during centrifugal motion. The calculation formula for centrifugal force is as follows:

$$F = mv^2 r \quad (2)$$

In formula (1-2), F - centrifugal force/(N); m - Quality of conveying medium/(Kg); r - The radius of centrifugal motion/(m)); v - Speed/(m/s).

Table 2. Influence of Vortex Chamber Diameter on Fluid Characteristics of Turbocharger

Title	Model 1#	Model 2#	Model 3#	Model 4#	Model 5#	Model 6#
Active channel pressure/Pa	121000	113000	141000	156000	149000	170000
Outlet channel pressure/Pa	2420	1990	2800	1800	2070	2000
Axial inlet 1 pressure/Pa	-49000	-42000	-38000	-38000	-41600	-31900
Axial inlet 2 pressure/Pa	-60600	-47000	-77000	-68800	-66500	-66600
Active channel velocity/(m/s)	61	61	61	60.7	60.8	60.5
Exit channel velocity/(m/s)	35.2	35.6	36.3	36	36	35.5
Axial inlet 1 velocity/(m/s)	9.2	9.18	8.7	8.7	9.13	8
Axial inlet 2 velocity/(m/s)	11	9.7	12.4	11.7	11.5	11.5
Active channel flow rate/(m3/s)	0.00479	0.00478	0.0047	0.0047	0.0047	0.0047
Flow rate of outlet channel/(m3/s)	0.0062	0.00625	0.00638	0.00632	0.0063	0.0062
Axial inlet 1 flow rate/(m3/s)	0.00077	0.00071	0.00068	0.00068	0.00071	0.00062
Axial inlet 2 flow rate/(m3/s)	0.00081	0.000755	0.00096	0.00091	0.000897	0.000898
Efficiency (%)	15.4	14.4	17.7	16.5	16.8	15.3

From the above equations (2), it can be concluded that the magnitude of the centrifugal force is directly proportional to the mass of the fluid, its velocity, and the radius of rotation. This paper primarily investigates the influence of the vortex chamber diameter on its fluid transport efficiency. Through the optimization design of the vortex chamber and the analysis of CFD calculation results, the optimal size of the vortex chamber is determined. The fluid characteristic parameters of different models of the vortex chamber supercharger are shown in Table 2. As the diameter of the vortex chamber increases, the working efficiency of the vortex chamber supercharger first increases and then decreases, with the maximum working efficiency reaching 17.7%.

4.3 Fluid Motion Characteristics

As shown in Figure 4, the fluid motion trajectories inside different vortex chamber models (Model 1#, Model 3#, and Model 4#) are illustrated. Fluid is drawn into the vortex chamber through the inlets on both axial sides. Under the influence of internal fluid motion, the fluid trajectories form a spiral shape and create a vortex in the central region of the vortex chamber. The fluid then exits through the tangential outlet of the vortex chamber under the action of centrifugal force. In contrast, Model 2# exhibits distinct upward and downward motion trajectories of the fluid drawn into the vortex chamber through the axial inlets, primarily due to the convective patterns at the inlets on both sides of the axis. No vortex phenomenon is observed in the vortex chamber of Model 2. As shown in Table 2, the average inflow velocity at the axial inlets of Model 2 is 9.44 m/s, which is the lowest among all models. This is likely the main reason for the lower efficiency of Model 2. In Model 3#, a significant vortex phenomenon occurs in the region deviating from the center of the vortex chamber, forming a distinct low-pressure zone and increasing the fluid velocity at the axial inlets. As shown in Table 2, Model 3# has the highest average inflow velocity at the axial inlets, reaching 10.55 m/s, which is the primary reason for its higher working efficiency. The fluid motion trajectory in Model 4# is similar to that of Model 3#, but the fluid motion in the axial region of the vortex chamber is relatively more complex. The vortex phenomenon in Model 4# shows

spatial layering and lacks concentration, mainly because the increase in vortex chamber size expands the region where vortices form but reduces the energy concentration of the vortices.

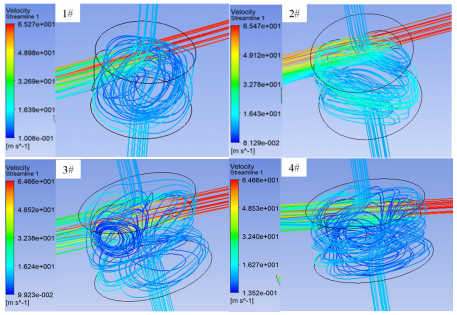

Figure 4. Fluid Motion Trajectories in Different Vortex Chamber Models

As shown in Figure 5, the numerical simulation of the fluid motion characteristics in the vortex chamber is presented. Figure 5(a) displays the pressure and velocity contours of the fluid inside the vortex chamber of Model 3#. The pressure in the vortex chamber is primarily distributed in the circumferential edge region, while a low-pressure zone forms in the axial center region due to the vortex effect. The fluid velocity in the vortex chamber follows the pressure distribution pattern, with the edge fluid velocity being higher than that in the axial region. The fluid velocity in the edge region of the vortex chamber is relatively uniform.

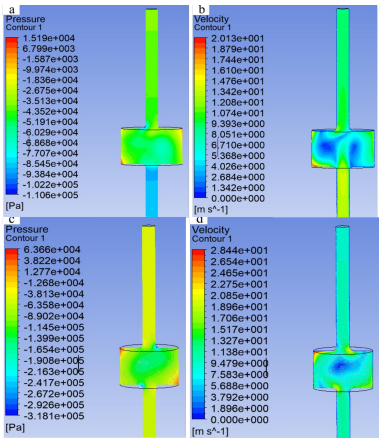

Figure 5. Numerical Simulation of Fluid Motion Characteristics:
(A) The Fluid Pressure Distribution Inside the Vortex Chamber of Model 3 #;
(B) The Fluid Velocity Inside the Vortex Chamber of Model 3 #;
(C) The Fluid Pressure Distribution Inside the Vortex Chamber of Model 2 #;
(D) Fluid Velocity in the Vortex Chamber of Model 2 #

Figure 5(b) shows the pressure and velocity contours of the fluid inside the vortex chamber of Model 2#. The pressure in the vortex chamber is mainly distributed in the diagonal edge regions, which aligns with the fluid velocity distribution. A small region within the vortex chamber exhibits very high fluid velocity, reaching up to 28.44 m/s. However, the fluid velocity in the edge regions of the vortex chamber is relatively low, and the overall fluid velocity inside the vortex chamber is unstable. Combined with the fluid motion trajectory of Model 2#, it is observed that no significant vortex phenomenon occurs inside the vortex chamber of Model 2#. The high-pressure zone along the diagonal is caused by the initial high-speed fluid from the tangential inlet flowing diagonally, without forming a distinct swirling vortex along the inner edges of the vortex chamber. This is the main reason for the lower average inflow rate at the axial inlets and the reduced working efficiency of Model 2#.

5. Conclusion

This paper establishes models of superchargers with vortex chambers of different diameters. Using FLUENT simulation software, the fluid domain is meshed and numerically simulated to obtain the internal fluid velocity, pressure distribution, and motion trajectories of different models. By analyzing the characteristics of fluid motion within the vortex chamber, the following conclusions are drawn:

(1) Fluid is drawn into the vortex chamber through inlets on both axial sides. Under the influence of internal fluid motion, the fluid trajectories form a spiral pattern, creating a vortex in the central region of the vortex chamber. The fluid then exits through the tangential outlet of the vortex chamber under the action of centrifugal force.

(2) As the diameter of the vortex chamber increases, the efficiency of the supercharger initially increases and then decreases. When the vortex chamber diameter is 50 mm, a distinct vortex phenomenon appears near the central region of the vortex chamber, forming a noticeable low-pressure zone. This enhances the fluid velocity at the axial inlets, with the maximum average velocity at the axial inlets reaching 10.55 m/s. Under these conditions, the highest efficiency achieved is 17.7%.

(3) The pressure and fluid velocity within the vortex chamber are primarily distributed in the circumferential edge region. The axial central area forms a low-pressure zone due to the vortex effect. The fluid velocity at the edges is higher than that in the axial region, and the fluid velocity in the edge area of the vortex chamber is relatively uniform.

Acknowledgments

This paper is supported by Key Research Project of Anhui Provincial Universities (No.2023AH051390); College Student Innovation; Entrepreneurship Training Program (No.202310375001); Research on Structural Optimization Simulation Design of Vortex Chamber Boosting Pump Model (No.hxkt2024385) .

References

[1] Yan Jinwen. Pump and Pump Station. Machinery Industry Press, 2008:6-25.

[2] Pang Hongmin. Research on Marketing Strategy of Grundfos Pump in China. Northeastern University, 2009:10-40.

[3] Chen Maoqing, Fan Mei. Performance of Self priming Centrifugal Pump for Transporting Viscous Liquids. Petroleum Machinery, 1992, 20(6):6.

[4] Zhang Zhan, Zeng Jianfeng, Xing Huaiyang. Design and Application of Pumps. Machinery Industry Press, 2015:6-45.

[5] Zou Wenlang. Performance Analysis and Experimental Study of Gas Liquid Two Phase Flow in Horizontal Self priming Pump. South China University of Technology 2023:10-60.

[6] Yang Sheng The Application of Pumps in the Petrochemical Industry. General Machinery, 2007(06):11-11.

[7] Calderón-Hernández W J, Sinatora A, Melo D G H, et al. Hydraulic convey of iron ore slurry: Pipeline wear and ore particle degradation in function of pumping time. Wear,2020,450-451.

[8] Staddon P. Sealless pumps for corrosive substances. World Pumps, 2005, 2005(468): 46-47.

[9] Tse P W, Wang D. Enhancing the abilities in assessing slurry pumps' performance degradation and estimating their remaining useful lives by using captured vibration signals. Journal of Vibration and Control, 2017, 23(12): 1925-1937.

[10] Wang Changbin, Bu Pingting, Zhi Shujie, et al. Numerical simulation of optimal throat distance for jet pump based on PHOENICS. Journal of Daqing Petroleum Institute, 2009, 33 (01): 41-44+77+121

[11] Sun Rui. Structural optimization design and hydraulic performance analysis of high-pressure rotary vane pump. Northeast Petroleum University, 2021:12-50.

[12] Gao Yang. Application of Liquid Gas Jet Pump Technology in Gas Boiler Flue Gas Waste Heat Recovery. HVAC, 2020, 50 (04): 75-78+20.

[13] Rogovyi, A. Energy performances of the vortex chamber supercharger. Energy, 2018, 163(15):52-60.

[14] Rogovyi A , Korohodskyi V , Medvediev Y , et al. Influence of Bingham fluid viscosity on energy performances of a vortex chamber pump. Energy, 2018, 218(1): 119432.1-119432.12.

